A methodology to capture the single blade loads on a cross-flow tidal turbine flume model

Timo BENNECKE, Shokoofeh ABBASZADEH, Karla RUIZ-HUSSMANN, Paul JOEDECKE, Pierre-Luc DELAFIN, Christian-Toralf WEBER, Stefan HOERNER

Abstract—**The OPTIDE project aims to improve the efficiency and durability of hydrokinetic cross-flow tidal turbines (CFTT). CFTT are attractive for the exploitation of tidal energy, because of high area-based power densities of such turbine arrays, a simple design and the ability to operate under varying flow conditions. Nevertheless, the efficiency of single CFTT is lower relative to the most commonly used axial turbine type. Furthermore the life time is often limited due to alternating and pulsating stresses. A promising approach to overcome these drawbacks is intracycle blade pitching. In this case the angle of attack is continuously adjusted individually for each blade during the rotation. The project aims to explore the influence of active blade pitching on CFTTs and to optimize it by numerical and experimental means. Therefore, a lab-scaled three-bladed experimental turbine with embedded pitch actuators is developed. The turbine is equipped with multiple full-bridges of strain gauges for the detection of tangential and radial components of the blade loads, from which the structural stress is calculated subsequently. To ensure the turbines mechanical durability, weakly coupled fluid-solid-interaction (FSI) simulations have been performed. Additionally, the FSI simulations show that a setup with strain gauges on a single blade support only allows for the measurement of the radial blade load component, as the measurements are distorted by pitching moments and secondary force paths. A revised instrumentation setup is developed and presented. The FSI simulations are adapted, to prove the suitability of the revised setup.**

Index Terms—**fluid-structure interactions, vertical-axis turbines, cross-flow tidal turbines, experiments, finite element analysis, instrumentation.**

Part of a special issue for EWTEC 2023. Original version published in EWTEC 2023 proceedings at https://doi.org/10.36688/ewtec-2023-501.

Manuscript submitted 10 January 2025; Accepted 2 May 2025. Published 31 May 2025.

This paper has been subject to single-blind peer review by a minimum of two reviewers.

This work is part of the OPTIDE project, supported by Deutsche Forschungsgemeinschaft (DFG (FKZ: 457325924)) and the labex Tec21 Investissements d'avenir - agreement n°ANR-11-LABX-0030.

T. Bennecke is researcher at the Laboratory of Fluid Dynamics and Technical Flows, Otto-von-Guericke-University Magdeburg, Universitätsplatz 2, 39106 Magdeburg, Germany (e-mail: timo.bennecke@ovgu.de)

K. Ruiz-Hussmann and S. Hoerner are affiliated at both the Laboratory of Geophysical and Industrial Flows (LEGI), CNRS, Grenoble-INP, University Grenoble-Alpes, France and the Laboratory of Fluid Dynamics and Technical Flows, Otto-von-Guericke-University Magdeburg, Universitätsplatz 2, 39106 Magdeburg, Germany (e-mail: karla.ruiz@ovgu.de, stefan.hoerner@univ-grenoble-alpes.fr)

S. Abbaszadeh is with Chair Electrical Drive Systems, Otto-von-Guericke-University Magdeburg, Universitätsplatz 2, 39106 Magdeburg, Germany (e-mail: shokoofeh.abbaszadeh@ovgu.de)

P. Joedecke was at the University of Applied Sciences, Department of Engineering and Industrial Design, Magdeburg, Germany (e-mail: paul.joedecke@guest.h2.de).

P.-L. Delafin reserches at the Laboratory of Geophysical and Industrial Flows (LEGI), CNRS, Grenoble INP, Univ. Grenoble Alpes, Grenoble, France (e-mail: pierre-luc.delafin@univ-grenoble-alpes.fr).

C.-T. Weber is currently at the University of Applied Sciences, Department of Engineering and Industrial Design, Magdeburg, Germany (e-mail: christian-toralf.weber@h2.de).

Digital Object Identifier: https://doi.org/10.36688/imej.8.197-206

I. Introduction

CLIMATE change demands a significant transition of the energy sector away from carbon driven fossil fuels towards renewable energy sources as far and fast as possible. Following the introduction of the European Green Deal in December 2019, the European Union (EU) developed a strategic plan for a carbon-neutral economic bloc by 2050. This ambitious road map includes a substantial reduction in greenhouse gas emissions (40%) in 2030 by increasing the contribution of renewable energy shares to at least 32% of the EU's total energy consumption[1]. The European Strategic Energy Technology Plan has set cost-reduction targets and suggests a deployment of 100 MW by 2025 and 1 GW by 2030 for wave and tidal energy[2].

In addition to achieving the European 2050 renewable energy goals, an unresolved challenge is to maintain grid stability, when accounting for the rising contributions of solar and wind energy as stated by Kyesswa *et al.* 2020 [1] or Urbanek *et al.* 2019 [2]. These are volatile power sources and cannot easily replace base load technologies fueled by coal and other fossil or nuclear resources.

In this context the use of tidal energy has the significant advantage that tides are fully predictable and largely unaffected by weather and climate change, since they mainly depend on planetary and lunar motion. Tidal, wave and marine flows represent the largest sources of renewable energy globally and thus can serve as clean and sustainable energy source due to their abundance and predictable nature as stated by Holzmann *et al.* 2007 [3], Angeloudis *et al.* 2016 [4] or Neill *et al* 2018 [5].

Conventional hydropower plants require a high degree of flow control and therefore structures to adjust the flow for the turbines as pointed out by Allmer *et al.* 1999 [6]. These systems fully control the flow

[1]https://climate.ec.europa.eu/eu-action/european-green-deal/2030-climate-target-plan_en

[2]https://setis.ec.europa.eu/implementing-actions/ocean-energy_en

conditions using a dam, accumulate a hydraulic head and concentrate the inflow to the turbine by a channelized inlet and guiding vanes. They are therefore able to operate at best point conditions for most operating scenarios. However this translates in high investments and impacts the environment in the long term.

Therefore novel technologies that adapt to the existing environmental conditions are needed to preserve natural resources and biodiversity but allow to exploit these new sources of energy in a sustainable matter.

Unlike traditional tidal hydropower technologies, such as the *La Rance* tidal power facility, which is based on a huge dam structure, which blocks and controls the water level of an entire estuary, hydrokinetic energy converters employed for tidal streams are installed directly in the sea to *harvest* the in-stream energy. This makes them an excellent candidate for sustainable energy exploitation.

This concept makes guiding structures or dams unnecessary and seems very promising for a sustainable exploitation of marine energy, as it leads to a very low ecological impact and minimal installation costs. However it comes with systemic challenges: the flow features no or only a negligible hydraulic head and the machine has to adapt to highly varying flow conditions. Therefore, it has to be able to operate under a large bandwidth of unsteady conditions.

A physical constraint, the so-called Lancaster-Betz-Joukowsky limit, forces these machines not to exceed 59% of the already small power portion of a free stream. This is due to a lack of any hydraulic head. However, the concept inherits an additional technical paradigm shift. Hydrokinetic energy converters make use of the instantaneous flow condition as it is, as they do not have any flow augmentation or control systems. In consequence their power coefficient (C_P), the dimensionless share of the extracted power commonly remains significantly lower than the physical limitations would allow.

Highly adaptive machines are necessary to reach at least the already small efficiency rates which are physically attainable. Possible measures can be active and passive flow control mechanism on blade level, such as demonstrated by Scholz *et al.* 2018 [7], Abbaszadeh *et al.* 2019 [8], Delafin *et al.* 2021 [9], Hoerner *et al.* 2021 [10] or most recently by Fasse *et al.* 2023 [11]. As an alternative, sophisticated rotor control methods and strategies such as shown by Strom *et al.* 2017 [12] can be employed. These methods allow for a device that operates under a broadest bandwidth of operating conditions and is both efficient and cost-effective.

In contrast to axial turbine types, mostly denoted by their horizontal rotor axis as horizontal axis turbine (HAT) which are commonly employed in wind industry, cross-flow tidal turbines (CFTT) also known as vertical axis turbines can feature higher area based energy densities in farm installations. This has been initially predicted by Whittlesey *et al.* 2010 [13] and validated in subsequent field tests by Dabiri 2011 [14]. These effects are considered to be a consequence of a lesser impact from frequent and instantaneous changes of the flow conditions to the power output and according to Brownstein *et al.* 2016 [15] in particular from positive inter-turbine interactions.

Unfortunately CFTT feature complex flow conditions in their rotor and suffer from flow-induced vibrations and alternating blade loads. The flow regime in the rotor is dominated by alternating flow separation and reattachment as a function of the rotor angle ϕ. This unsteady flow leads to a rather poor single turbine efficiency compared to their axial competitors.

In terms of the OPTIDE project, which is subject to this study, an active flow control methodology on blade level is investigated. The angle of attack α is directly controlled by an active pitch motion of the blade, which allows to mitigate and suppress such a flow separation and in consequence dynamic stall. The aim is to achieve an optimal pitch trajectory from experiments. It is hypothesized to be a trade-off in between a sufficient high angle of attack α to generate the highest possible torque resulting from the lift forces but at the same time α has to remain below a critical stall angle to avoid a fully separated flow. A stalled flow would lead to a loss of any lift and a sharp increase of the drag on the blade and therefore critically impact the power output.

An optimized pitch trajectory would combine a maximized rotor efficiency with minimized structural loads to avoid fatigue failure and increased material use. This aim requires an experimental flume model with complex instrumentation.

In a first step of the development of such a down scaled flume model, numerical means were employed to estimate the best blade design with use of a systematic shape optimization prior to the experiments, using the methods introduced by Ruiz-Hussmann *et al.* 2022 [16] and 2023 [17]. They were accompanied by parallel weak-coupled fluid-structure interaction simulations as already presented by Bennecke *et al.* 2022 [18] to support the model turbine design and the instrumentation of the rotor. The impact of the rotor geometry and the complex fluid-solid-interactions to the instrumentation design is subject to the study at hand and will be shown subsequently.

II. Methodology

In the following, a short overview of the applied methodology is provided. After briefly presenting the boundary conditions and the experimental turbine, the experimental setup for the measurement of the blade forces is described in detail. Then numerical simulations based on the real conditions are summarized and the integration of this setup into the numerical turbine model is shown.

A. Turbine geometry and experimental enviroment

The experimental turbine model, subsequently denoted as *flume model*, will operate in a laboratory flume with a cross-section of 1200 $\times$ 600 mm² and with a channel flow speed of roughly 0.7 m/s. In a trade-off between Reynolds (Re) similarity and blockage ratio the diameter of the turbine was set to 400 mm. A three-bladed design was chosen to minimize torque

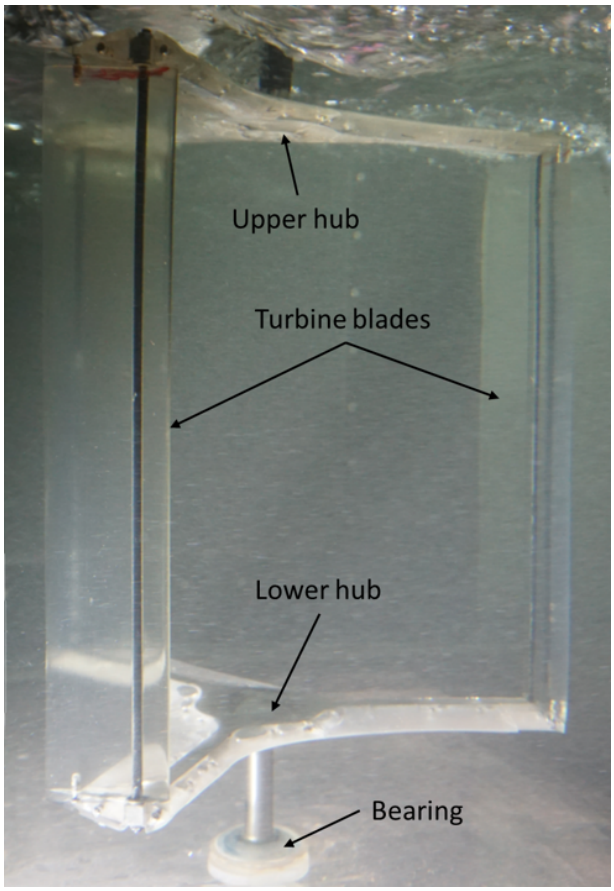

Fig. 1. Scaled model of a CFTT in the laboratory flume, which is used in the project. Fixed turbine blades with symmetrical NACA 0018 profile are mounted. (The original image was rectified in order to correct lens aberration effects)

ripples but still achieve a sufficiently high tip speed ratio (λ) at the best point of operation. The blade length was determined with the definition of an aspect ratio and solidity $\sigma = \frac{nC}{R}$ to be roughly equal to 1, with n the number of blades, C the chord length and R the turbine radius. Thus a chord length of 70 mm is aimed resulting in an average Re of 120,000 at λ=2.00. For the general rotor design two supporting arms on the tips of the blades (O-design) were chosen to avoid flow disturbances in the most productive region of the blade, as it is the case for the H-rotor design. Furthermore, the tip-support structure has a winglet-like effect on the pressure distribution on the blades. Choosing a classical symmetric NACA0018 profile shape for the blades as a starting point before the aforementioned shape optimization, the overall rotor design (as shown in Fig. 1) had been fully defined.

For sake of simplicity the turbine concept is based on an aluminum based skeleton (material EN ISO AL-6061 T6) from standardized parts and simple geometries such as rectangular cross-sections and water jet cut plates. In order to achieve a flow adapted design the shape of the turbine was realized by a 3D printed shell structure (printed from clear resin with a Formlabs 3L printer) which allows for a fast uptake of design changes with low costs and minimal effort. In particular the strength, mass, inertia and rigidity of the structure is mostly unaffected by changes of the outer

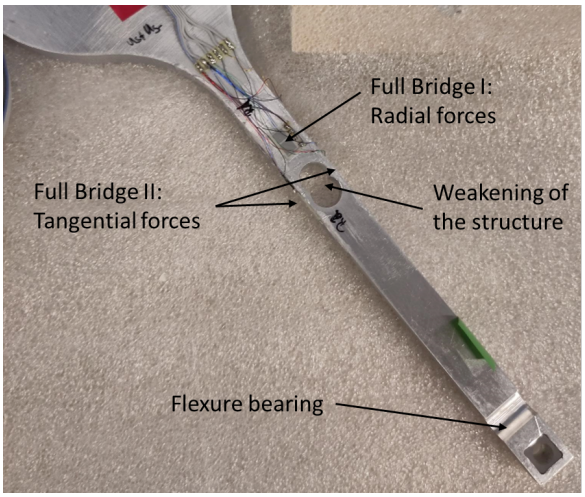

Fig. 2. Design and instrumentation of the rotor: one strain gauge, mounted to one strut of the upper hub. The visible strain gauge is part of the full bridge for the measurement of the radial force component. It consists of two 3 mm $\times$ 3 mm measuring elements. Also visible is the weakening for the tangential force measurement and the solid state joint next to the blades mounting point

body shell, which makes different designs comparable in between each other.

The drag of the hubs influences the characteristics of the turbine and should therefore be reduced. To do so, fairings with an aerodynamic, symmetrical profile are used. The profile resembles a NACA-0018 profile without inclination, which is adapted in its size to the cross-squared section of the hubs' struts. The transition between the blade and the fairing of the hub is rounded by an additional endcap. Since a symmetrical profile is used, it is assumed that all other hydraulic forces than the drag acting on the support structure are negligibly low.

The flume setup comprises a position controlled drive system (power inverter Kollmorgen AKD-P00306 with Siemens 1fk7042-5af71-1ta0) as load for the prime mover which allows to perform not only a rotational speed from 0-150 rpm but also to achieve variable speed during a rotor turning cycle. A torquemeter (Lorenz Meßtechnik FM-G 30 NM) installed in between drive and turbine allows for a determination of the mechanical torque. The position feedback from the drive system is captured as a soft signal in quadrature mode with a LabjackT7 acquisition card governed as well as the drive system using an extended version of the customized Python environment running on a Linux desktop system, as introduced by Abbaszadeh *et al.* 2019 [8] and Hoerner *et al.* 2019 [19].

The aim of the experiments, the definition of an optimized pitch trajectory as a trade-off of turbine efficiency and structural loads, requires the knowledge of the instantaneous torque and the synchronized explicit single-blade loads. While the first is measured with the aforementioned system, the latter will be achieved by the use of strain gauges in a customized setup.

B. Experimental setup

The flume model is dedicated to serve for an investigation of the impact of active pitched blades and

the validation of numerical studies in particular on suitable blade shapes in CFTT. In consequence evaluating rotational speed, torque and C_P is not sufficient, because the alternating radial force component which mainly impacts on the turbine's service live would remain unknown. Therefore, the instrumentation was extended by strain gauges added at the metal based support structure, which connects the turbines blades with the central shaft of the turbine (see Fig. 2).

The suitability of the chosen setup had to be proved during the design process. Aim was that the strain of the strain gauges should be directly and only dependent on the blade forces.

Two major assumptions were made for the design of the flume model:

1) Force paths that transmit the tangential forces (torque) from one to the other blades via the lower hub, which is not connected to the load machine, are small and can be neglected.
2) Symmetrical NACA0018 profiles are used. These are assumed to be free of a pitching moments at quarter chord in accordance to classical airfoil theory. In consequence the pitching moment on the blade can be neglected.

As described in sec. II-A, the flume model consists of a three-bladed rotor, which is supported by two ball bearings placed above and below the turbine. The torque generated by the turbine is transferred to the load machine above the upper bearing via a flexible coupling to the torquemeter. No central shaft, which connects the lower and upper hub, was used in the first design shown in Fig. 1. It was considered that a central shaft would interact with the flow inside of the turbine and therefore reduce the power coefficient (C_P).

Strain gauges employed as full bridges are used for the determination of the blade forces. The full bridges suppress or better balance any changes of the resistance resulting from loads in all directions other than the one of interest. Thus, the change in resistance is linearly related to the direction of deformation, which results from a force in a single axis. In the case of the flume model, deformation and resistance change from the tangential and radial forces are measured separately by use of two full bridges. To this purpose the latter were bonded to the struts which are connecting one rotor blade with the turbines shafts.

The orientation of the strain gauges as well as their position is shown in Fig. 3. Full bridge I, displayed in Fig. 3 and Fig. 2, is consisting of two T-rosette strain gauges, which are bonded to the upper and lower side of one strut of the upper hub. The radial force is determined from the measured strain by means of the Young's modulus of the material and the cross-sectional area of the strut. Full bridge II, also visible those figures, is made of two dual-grid strain gauges, mounted to the sides of the strut. This second full bridge measures the strain from the bending stress in the material, which is caused by the tangential force and the distance between the bridge and the center of the profile. Close to the bridges, a terminal is used for the interconnection of the strain gauges and as a transition to firmer cables leading out of the turbine to a

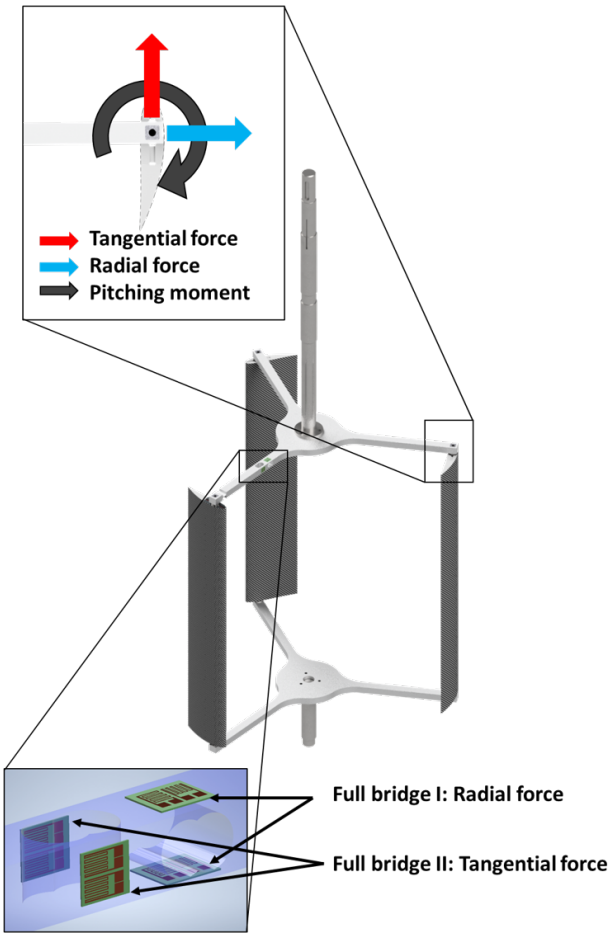

Fig. 3. Blade force components and strain gauge layout: The turbines' model is displayed without the fairing of the hubs.The displayed blades are covered by a 0.25 mm carbon layer which will be added to the blades in the future. The carbon layer is also taken into account for the FSI, as presented by Bennecke [18].

micro controller. The voltage supply of all strain gauges is done using two cables, one for + and one for -, which are subsequently further distributed to feed all strain gauges of the setup. The output voltage of the full-bridges (the signal) is directly connected to the micro controller outside of the turbine placed on a rotating platform. To tap this voltage, the corresponding strain gauges of Full Bridge I are connected directly on the carrier-layer. The wiring of the strain gauges is carried out according to the manufacturer's instructions.[3]

To adapt the strain to the measuring range of the used strain gauges, the struts are weakened in the area of the strain gauges. The mounted strain gauges are displayed in Fig. 2.

In addition to the strain gauge full bridges, flexure bearings are used for a decoupling of the strut from the bending moment, which is caused by a possible bending of the rotor blades during operation. Without this measure, strains caused by superimposed bending moments could not be distinguished from the strain caused by the radial forces. The flexure bearing is also visible in Fig. 2. Only one blade has been decoupled in order to not reduce the rigidity of the turbine more than absolute necessary.

[3]https://www.me-systeme.de/en/technology-first/strain-gauge/wiring-diagrams

TABLE I
HARDWARE COMPONENTS

Strain gauges	Axial force	Tangential force
Type	T-Rosette	Dual-Grid
	X-TA1XK3	X-DA1XK3
Provider	ME-Messsystem	ME-Messsystem
Length × width	7.5mm × 9.1mm	7.3mm × 8mm
k-Factor	2.0	2.0
Resistance R	350 Ω	350 Ω
Grid size	3mm × 3mm	3mm × 3mm
Measuring range	-300 to 300 μm/m	-300 to 300 μm/m
Signal amplifier		
Operational amp	OPA344	Texas Instrument
Gain	1000	
Coefficient of determination (R^2)	0.98	0.99
Micro controller		
Type	F28069	Texas Instrument

Voltage signals from the strain gauges are measured by means of a custom signal amplifier connected to a microcontroller TI-F28069 provided by Texas Instruments. The microcontroller discretizes the input voltage of 0 to 3.3 V with 16 bit resolution (0 to 2048 bits). The full bridges are operated with 3.3 VDC. The output voltages are amplified by a gain factor of 1000 and processed by the microcontroller. The specifications of the materials employed can be found in Table I.

Preliminary calibration test were carried out. For this purpose, the clamped hub structure was radially and tangentially loaded with a reference force gauge (Sauter FC-10). The load was initially increased to 10 N in 2 N steps and then reduced again. All values have a tolerance of ±2 bit due to electrical noise. For a load change of 0.417 N on average, the output changes by one bit. In Fig. 4 and Fig. 5 the results of the calibration tests are shown. On the abscissas, the applied force is indicated in N. The ordinates are providing the amplified full bridge voltage signal in bits. In addition, the linear relationship between radial force and output is checked by means of a linear regression. The regression line is drawn as a dashed line and the coefficient of determination (R^2) value is calculated. The uncertainty, consisting of the fluctuations of the output (±2 bits), the tolerance of the force gauge (±0.02 N, corresponding to approx. 0.048 bits) and the minimum measurable force change (±0.5 bits), is colored gray in figure 4, which proves a very good repeatability and low scattering in measurements.

C. Numerical models

Prior to the manufacturing of the turbine flume model, the structural stability of the model has been verified, using a weak coupled fluid structure interaction (FSI) simulations. The numerical modeling of the flume model, subsequently denoted *FSI model*, was implemented using a combination of the open source toolbox OpenFOAM (ESI fork v2112) and the proprietary software package Ansys Workbench (2020 R2). In a 2D unsteady Reynolds-averaged Navier-Stokes (URANS) simulation (OpenFOAM) of the turbine, the instantaneous chord wise pressure distribution was calculated. This set of data corresponds to a cross

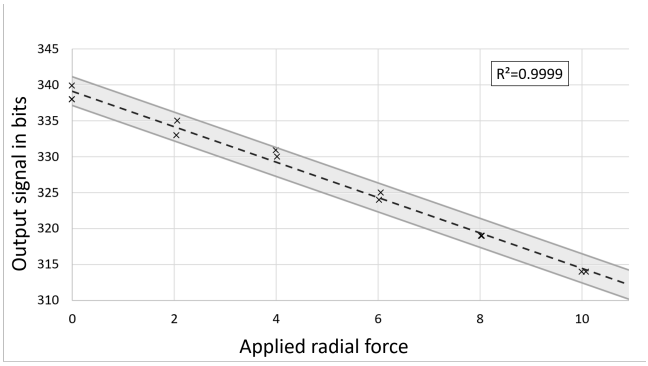

Fig. 4. Calibration test of the radial force full bridge. The abscissa displays the applied force in N. The ordinate provides the amplified output voltage signal in bits. Colored in gray is an area of uncertainty, which is caused by the magnitude of the smallest detectable variation.

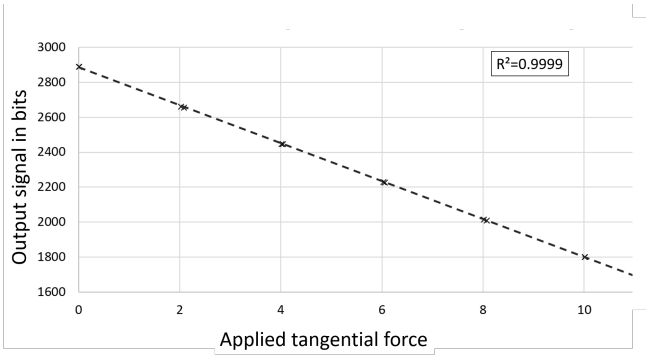

Fig. 5. Calibration test of the tangential force full bridge. The abscissa indicates the applied force in N. The ordinate provides the amplified output voltage signal in bits.

section representative of the middle of the blade (symmetry plane of the rotor, also called equatorial plane), where 3D effects are not significant. This 2D pressure-distribution, consisting of 36 discrete load steps (one for each 10°) forming one full rotation was subsequently transferred to a finite element analysis (FEA, Ansys Workbench) using ASCII-Files (.txt). For the 3D rotor geometry, a 3D pressure distribution was created by uniformly sweeping the 2D distribution along the blade length and mapping it onto the rotor blades of the FEA model. In the last step, a 3D transient FEA analysis for the 36 load steps was performed to determine stresses and loads of the structure.

For the validation of the coupling strategy, the torque coefficients calculated once by the means of the CFD results ($C_{\mathrm{T,CFD}}$), and in the second case calculated from the turbines torque reaction in the FEA ($C_{\mathrm{T,FEA}}$) were compared. The mean values of the coefficients with 0.3313 ($C_{\mathrm{T,CFD}}$) and 0.3307 ($C_{\mathrm{T,FEA}}$) showed very good accordance with an average deviation of 0.19 %. Details of the setup and the FSI model can be found in Bennecke *et al.* 2022 [18].

It is obvious that the coupling of a 2D-CFD analysis with a 3D FEA structural analysis for the design of a CFTT only roughly approximates the real flow conditions. Drag losses, blade tip losses and the influence of the hub on the flow are neglected, which will lead to an overestimation of the real blade loads, as well as the

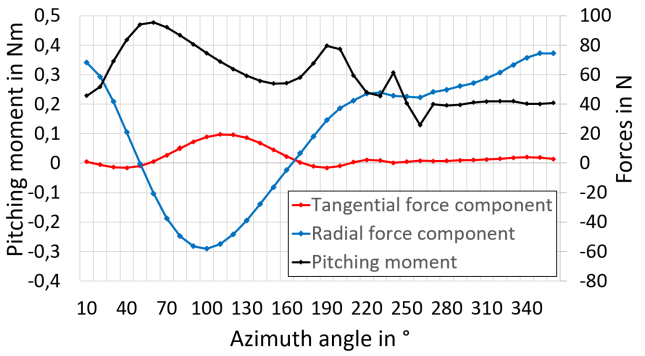

Fig. 6. Blade force components in [N] (right abscissa), and the pitching moment around the aerodynamic center of the blade ($0.25C$) in [Nm] (left abscissa). The ordinate shows the azimuth angle over one full rotation in [°] for the flume model (400 mm diameter and blade length, with 3 NACA0018 hydrofoils projected onto the turbine perimeter). The simulated flow speed is 0.7 m/s and $\lambda = 2.25$.

expectable C_P. According to Villeneuve *et al.* 2021 [20], the height of the overestimation depends strongly on the turbines layout as well as the design of the hub and can thus not be estimated with the existing knowledge. Furthermore, the numerical simulation of the flow conditions for a CFTT is challenging. In particular dynamic flow separation of the boundary layer and subsequent reattachment can hardly be simulated with commonly used URANS approaches which makes use of significantly simplified turbulence models. However, the cycle-averaged C_P can be estimated with satisfying accuracy in the best point, as shown by Ferreira *et al.* 2007 [21], Maître *et al.* 2014 [22] or Daróczy *et al.* 2015 [23]. In summary, it has to be assumed that both the performance of CFTT as well as the hydrodynamic loads are probably overestimated using the current approach. However, this was considered to provide a systematic *security margin* for the design of the flume model. Furthermore, there are indications that mainly the tangential force components are affected, as described by Li *et al.* 2013 [24].

The numerical model allows for the determination of the variation of the blade force components during a rotor cycle, the driving tangential component, the radial component, and the pitching moment.

The development of the blade loads for one blade over a rotor cycle at the best point of operation ($\lambda = 2.25$) is shown in Fig. 6. Overall, the simulated blade loads are in good accordance with simulations done by Li *et al.* 2013 [24] and Bianchini *et al.* 2016 [25].

The strain gauges are integrated into the FSI model through the definition of their base area in the FEA. The base area, as given in the corresponding data sheets, is used, because homogenization effects due to adhesive layers and carrier materials are not taken into account any further. Numerical *sensors* were added, which are detecting the radial strain in the defined surface areas. Resistance changes of the strain gauges resulting from strains in other directions are completely compensated by the full bridges or within a measuring grid and can therefore be neglected in the FSI model. In the

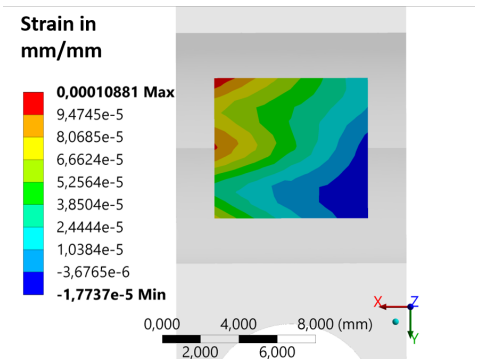

Fig. 7. The radial strain in the base area of a strain gauge for the detection of the radial force component at an azimuth angle of 360° (after one rotation) is shown in mm/mm.

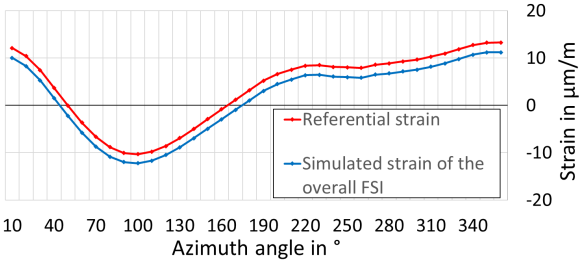

Fig. 8. Referential strain from a single blade load with radial forces (red) and strain captured under full load from three blades (blue). The abscissa displays the turbine's azimuth angle over one cycle, and the ordinate the averaged strain over the strain gauges base areas in [µm/m].

following, strain always refers to an *averaged* strain over the unevenly deformed base area of the respective strain gauge, as visible in Fig. 7.

The averaged strain is used due to the neglect of the relation between stress, strain, and resistance changes of the strain gauges, which is known only approximately. To estimate a measurement error caused by the elasticity of the turbine, the comparison of the strain with expected values is sufficient.

III. Results and Discussion

Following the assumptions made in sec. II-B, two full brigdes of strain gauges were used in the first setup. One bridge is dedicated to the detection of radial strains, as a result of the radial component of the blade loads, and a second pair for the detection of the bending moment on the support caused by the tangential force component. The simulated strains for the strain gauge base areas over one cycle are displayed in Fig. 8 & 9. In these diagrams, the strain for the complete FSI model (blue solid line) is compared to the strain captured by a simulation of a single blade load deserving as the reference for the setup (red solid line). In the latter a FEA model of the isolated upper hub was calculated. Loads equivalent to those caused by the blade of interest are applied at the contacts to the hub structure from the full model.

A comparison of Figs. 6, 8 & 9 shows that only the radial force component can be investigated with the current setup. However, there is an offset in between

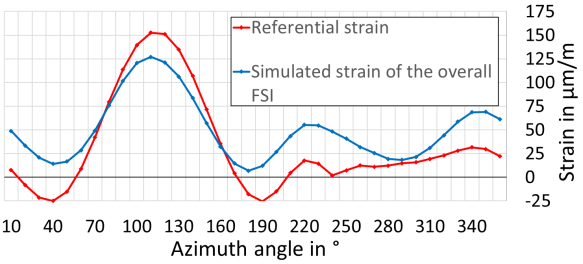

Fig. 9. Referential strain from a single blade load with tangential forces (red) and strain captured under full load from three blades (blue). The abscissa displays the turbine's azimuth angle over one cycle, and the ordinate the averaged strain over the strain gauges base areas in [µm/m].

the radial force and the strain of the strain gauges as depicted in Fig. 8. In contrast, the curves of the tangential force and the strain of the associated strain gauges, shown in Fig. 9, are not in accordance. Load peaks originating from the other blades can be found in the strain curves. Also the averaged value of the full load strain simulations does not fit within the expectations. A further investigation of the average strain which would be expected from the tangential force showed that this is with 31.65 µm/m significant lower than the strain found in the simulation, which is 49.64 µm/m. Taking the pitching moment into account, the difference between the averages drops from 17.99 µm/m to 4.56 µm/m, with an average strain of 45,08 µm/m.

The FSI model comparison with the single blade reference load clearly showed that the tangential force component of the blade cannot be captured with the model at hand. In consequence a revised setup was designed in order to account for the additional interfering loads from the other rotor blades.

A. Revised measurement setup

Two major problems were identified in the first instrumentation design:

1) secondary force paths
2) a non-negligible pitching moment

The first can be eliminated via additional measurements of the strain at the corresponding strut of the lower hub. For the calculation of the tangential force components, the mean value of the strains at the upper and lower hub could be used.

Nevertheless, a different approach is also possible and was privileged for the flume model. Due to already predictable future stiffness and rigidity problems arising from the use of blade-embedded brushless DC-motors (BLDC) for the pitching motion a central shaft has been added to the flume model. Pitch moment and tangential force are in consequence splitted evenly in between the lower and upper hub in the same way as the radial force component.

B. Retrieving the pitching moment

The second challenge of the previous setup was the existence of a non-negligible pitching moment. With

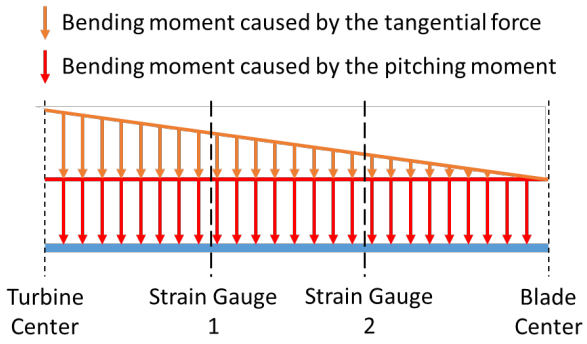

Fig. 10. Schematic curves of the superimposing bending moments over the length of the strut. The bending moment caused by the tangential force component (orange) and the moment caused by the pitching moment (red). Also marked are the two measuring points where the total magnitude of the combined bending moment is measured.

the two force components and the pitch moment, three unknown variables remain to be detected. Following, at least one additional sensor is required in order to built an analytic mechanical model to distinct in between the different load origins. Two different concepts for the integration of a third sensor were discussed:

I) Pitch moment sensing from embeded actuation: the pitching moment can be calculated from the electric current [A] of the embedded actuators as the machine torque is proportional to the current. The relation between the two is defined via the machine constant, which commonly given by the manufacturer. In this case the actuator would become a sensing device which is charming due to simplicity of the approach. However, since inaccuracies due to the friction and resistance from sealings and bearings, in particular due to different coefficients of static and dynamic friction are foreseeable, this approach was not pursued further.

II) Pitch moment sensing with strain gauges: the main problem in the former setup was the presence of two superimposed bending moments at the strain gauges:
   1) The first bending moment is caused by the radial force component. The moment trajectory starts with 0 N at the aerodynamic center of the blades profile, and increases linear up to its maximum at the turbine's center, as the strut is the lever.
   2) The second bending moment is caused by the pitching moment itself. It remains constant over the entire length of the strut. However, only the shape of this bending moments curve is known.

   Both moments superimpose each other. The curves of the combined bending moments over the length of the strut are displayed in Fig. 10. The strain at the surface is linearly dependent on the bending moment.

In consequence a second bridge of strain gauges can be used in order to measure the bending moment at two points along the strut. Due to the known linear behavior of the curve and the known geometry of

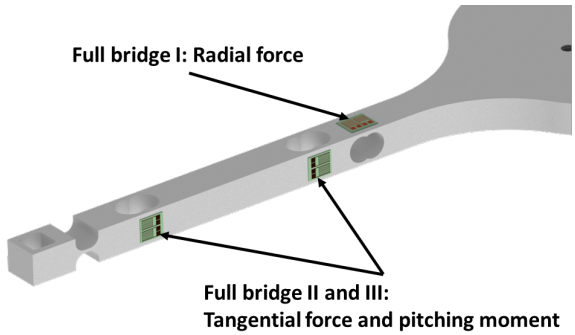

Fig. 11. Rendering of the upper hub with the proposed new strain gauge layout. Full bridge II and III are the implementation of strain gauge 1 and 2, which are marked in the schematic diagram Fig. 10. Full bridge I, for the detection of the radial load component, is also shown in Fig. 2 and Fig. 3.

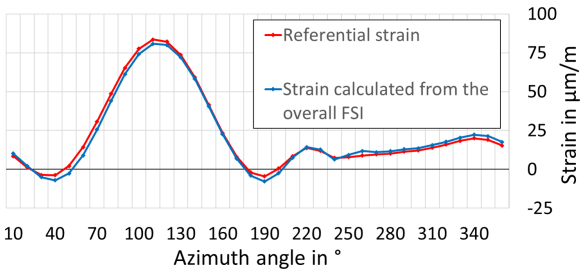

Fig. 12. Comparison of the reference strain (red), and the calculated portion of the strain caused by the tangential force in the FSI model (blue). Compared are the strains of strain gauge full bridge 1.

the turbine, the size of the bending moment at both ends of the strut as well as the constant (from pitching moment) and linear share (from tangential forces) can be calculated, while the size at the center of the blade represents the pitching moment. The tangential blade force component is calculated using the difference between the bending moment at the blade's shaft and the turbine's central shaft and subsequent division by the lever.

The addition of the second strain gauge full bridge, displayed in Fig. 11 has been validated with the FSI model, which has been extended by a continuous central shaft. Following, parts of the tangential force component are now transferred to the lower hub, and the expected force, which is transferred to the upper hub, is halved. Due to the linear relation between force, strain, and resistance change of the strain gauges, the expected strain is also halved. A comparison of the expected deformation caused only by the tangential force component with the deformation calculated with the help of the sensors in the complete FSI model can be seen in Fig. 12. Fig. 13 shows the component caused by the pitching moment.

C. Calculation of the error magnitude

As summarized at the beginning, strain gauges are needed for the detection of the single blade forces. The turbine's elasticity leads to an error effecting the relation between the real blade forces and the strain measurements on the strut. To reduce this error, the constant sensor offset, which corresponds to the average deviation, is subtracted. The offset will be eliminated prior to the experiments by calibration of the strain gauges on the fully assembled turbine with reference loads. The dynamic share of the error, which leads to a non-linear behavior of the relations in between force, strain, and subsequently resistance change of the strain gauges, cannot be corrected and is accounted for the evaluation of the sensor system accuracy. The magnitudes of these errors are listed in table 1.

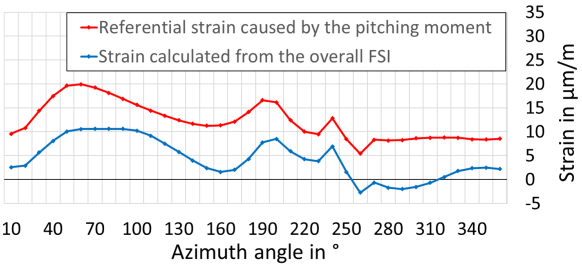

Fig. 13. Comparison of the reference strain (red), and the calculated portion of the strain caused by the pitching moment in the FSI model (blue).

TABLE II
ERROR MAGNITUDES CAUSED BY THE ELASTICITY OF THE TURBINE

Force component	Median of the error	Standard deviation
radial	0.046 µm/m,	0.048 µm/m
tangential	2.183 µm/m,	1.232 µm/m
pitching moment	1.563 µm/m,	0.723 µm/m

The Median of the error is referring to the difference between the reference strain and the strain found in the FSI model (after the removal of the constant offset).
The Standard deviation also refers to the error after the removal of the constant offset.

IV. Conclusion

Aim of this study is to validate the suitability of a instrumentation design for an experimental flume model turbine used in the OPTIDE project. It has been shown that the first design is not sufficient for the upcoming experiments, since the tangential part of the blade forces, which is driving the turbine, cannot be captured due to load interference from the other blades via the lower hub and a significant pitching moment on the blade.

To solve the problems mentioned above, the turbine design has been revised and extended by a continuous shaft. Blade forces are now transmitted equally through both hubs and interference from the lower hub is eliminated. An additional full bridge of strain gauges has been attached to the upper hub. With this addition and the original ones, the tangential force component as well as the pitching moment can be calculated using a simple analytical model.

It is shown, that the radial and tangential force component can be recorded precisely with the revised setup. The pitching moment can also be captured, but the accuracy of the result will be significantly lower due to the turbine elasticity.

The findings of the study are in good accordance to McLaren 2011 [26] for a similar setup on a vertical axis wind turbine. However, it has to be noted that the direct transfer of the research results from vertical axis wind turbines to CFTT is not possible without further ado, as described by Kirke and Lazauskas 2011 [27].

The developed turbine model design with the instrumentation for the detection of the blade forces, as well as the experimental data, which will be collected, can be used not only for the research in the OPTIDE project, but also for the validation and improvement of any numerical simulations of CFTT and will provide a valuable test bench for future studies on CFTT.

The presented measurement setup bears the drawback to be only suitable for the determination of blade forces on turbines with a continuous shaft joining upper and lower hub structure. However in order to investigate layouts without a continuous turbine shaft the design has been renewed: the hub position have been changed and the upper hub is now reused on the lower position. For the upper hub three additional full bridges have been installed. Assuming that the pitching moment is transferred approximately equally to both hubs, layouts without a central shaft can now be investigated with the given setup.

AUTHOR CONTRIBUTIONS

T.B.: Conceptualization, Methodology, Software, Validation, Data Curation, Formal analysis, Investigation, Writing - Original Draft, Visualization. **S.A.**: Methodology, Software, Investigation, Data Curation, Writing - Review & Editing **K.R.H.**: Investigation, Writing - Review & Editing. **P.J.**: Conceptualization, Methodology, Writing - Review & Editing. **P.L.D.**: Investigation, Resources, Data Curation, Writing - Review & Editing, Supervision. **C.T.W.**: Conceptualization, Resources, Supervision. **S.H.**: Conceptualization, Methodology, Resources, Data Curation, Writing - Review & Editing, Supervision, Project administration, Funding acquisition.

REFERENCES

[1] M. Kyesswa, H. Cakmak, U. Kuhnapfel, and V. Hagenmeyer, "Dynamic Modeling of Wind and Solar Power Generation with Grid Support for Large-Scale Integration in Power Systems," in *2020 IEEE PES Innovative Smart Grid Technologies Europe (ISGT-Europe)*. IEEE, 2020, pp. 569–573.

[2] S. Urbanek, D. Heide, B. Bagaber, M. Lohss, B. Specht, X. Paulig, A. Mertens, and B. Ponick, "Analysis of External Rotor Electric Drives for an All-Automatic Airborne Wind Energy System," in *2019 IEEE International Electric Machines & Drives Conference (IEMDC)*. Piscataway, NJ: IEEE, 2019, pp. 1599–1606.

[3] D. C. Holzman, "Blue Power: Turning Tides into Electricity," *Environmental health perspectives*, vol. 115, no. 12, pp. A590–3, 2007.

[4] A. Angeloudis, R. A. Falconer, S. Bray, and R. Ahmadian, "Representation and Operation of Tidal Energy Impoundments in a Coastal Hydrodynamic Model," *Renewable Energy*, vol. 99, pp. 1103–1115, 2016.

[5] S. P. Neill *et al.*, "Tidal Range Energy Resource and Optimization – Past Perspectives and Future Challenges," *Renewable Energy*, vol. 127, pp. 763–778, 2018.

[6] H. P. Allmer, "Combined discharge control of the hydropower plants on the Austrian Danube," in *1999 European Control Conference (ECC)*. IEEE, 1999, pp. 4887–4892.

[7] P. Scholz, V.M. Singh, A. Gebhardt, S. Löffler, and J. Weiss, "A Comparison of Different Active Flow Control Methods on a Generic Vertical Tail," in *Deutscher Luft- und Raumfahrtkongress*, 2018.

[8] S. Abbaszadeh, S. Hoerner, T. Maître, and R. Leidhold, "Experimental investigation of an optimised pitch control for a vertical-axis turbine," *IET Renewable Power Generation*, vol. 13, pp. 3106–3112(6), 2019.

[9] P.-L. Delafin, F. Deniset, J. A. Astolfi, and F. Hauville, "Performance improvement of a darrieus tidal turbine with active variable pitch," *Energies*, vol. 14, no. 3, p. 667, jan 2021.

[10] S. Hoerner, S. Abbaszadeh, O. Cleynen, C. Bonamy, T. Maître, and D. Thévenin, "Passive flow control mechanisms with bioinspired flexible blades in cross-flow tidal turbines," *Experiments in Fluids*, vol. 62, no. 104, pp. 1–14, 2021. [Online]. Available: https://link.springer.com/article/10.1007/s00348-021-03186-8

[11] G. Fasse, M. Sacher, F. Hauville, J.-A. Astolfi, and G. Germain, "Multi-objective optimization of cycloidal blade-controlled propeller: an experimental approach," *preprint*, 04 2023. [Online]. Available: www.researchgate.net/publication/369795243_Multi-objective_optimization_of_cycloidal_blade-controlled_propeller_an_experimental_approach

[12] B. Strom, S. Brunton, and B. Polagye, "Intracycle angular velocity control of cross-flow turbines," *Nature Energy*, vol. 2, 2016.

[13] R. Whittlesey, S. Liska, and J. Dabiri, "Fish schooling as a basis for vertical axis wind turbine farm design," *Bioinspiration & Biomimetics*, vol. 5, no. 3, p. 035005, 2010.

[14] J. Dabiri, "Potential order-of-magnitude enhancement of wind farm power density via counter-rotating vertical-axis wind turbine arrays," *Journal of Renewable and Sustainable Energy*, vol. 3, no. 4, 2011.

[15] I. Brownstein, M. Kinzel, and J. Dabiri, "Performance enhancement of downstream vertical-axis wind turbines," *Journal of Renewable and Sustainable Energy*, vol. 8, p. 053306, 2016.

[16] K. Ruiz Hussmann, P.-L. Delafin, C. Bonamy, Y. Delannoy, D. Thévinin, and S. Hoerner, "Blade shape optimisation of a vertical axis tidal turbine under constraints," in *Proc. Conference on Modelling Fluid Flow (CMFF'22) in Budapest, Hungary*, 2022, pp. 420–426.

[17] K. R. Hussmann, P.-L. Delafin, C. Bonamy, Y. Delannoy, D. Thévinin, and S. Hoerner, "Objective functions for the blade shape optimization of a cross-flow tidal turbine under constraints," in *Proceedings of the 15th European Wave and Tidal Energy Conference, 3–7 September 2023, Bilbao*, 2023.

[18] T. Bennecke, K. Ruiz Hussmann, P. Joedecke, C.-T. Weber, P.-L. Delafin, C. Bonamy, and S. Hoerner, "A weak coupled model for the fluid-structure interactions on cross-flow tidal turbine model," in *The 8th European Congress of Computational Methods in Applied Sciences and Engineering ECCOMAS Congress 2022, Oslo, Norway*, 2022.

[19] S. Hoerner, S. Abbaszadeh, T. Maître, O. Cleynen, and D. Thévenin, "Characteristics of the fluid–structure interaction within Darrieus water turbines with highly flexible blades," *Journal of Fluids and Structures*, vol. 88, pp. 13–30, 2019.

[20] T. Villeneuve, G. Winckelmans, and G. Dumas, "Increasing the efficiency of vertical-axis turbines through improved blade support structures," *Renewable Energy*, vol. 169, 01 2021.

[21] C. Ferreira, G. Bussel, van, and G. Kuik, van, "2d cfd simulation of dynamic stall on a vertical axis wind turbine : verification and validation with piv measurements," in *45th AIAA Aerospace Sciences Meeting 2007, 8-11 January 2007, Reno, NV*, 2007, pp. 16 191–16 201.

[22] T. Maître, E. Amet, and C. Pellone, "Modelling of the flow in a Darrieus water turbine: Wall grid refinement analysis and comparison with experiments," *Ren Energy*, vol. 51, pp. 497–512, 2013.

[23] L. Daróczy, G. Janiga, K. Petrasch, M. Webner, and D. Thévenin, "Comparative analysis of turbulence models for the aerodynamic simulation of h-darrieus rotors," *Energy*, vol. 90, pp. 680–690, 2015.

[24] C. Li, S. Zhu, Y.-l. Xu, and Y. Xiao, "2.5d large eddy simulation of vertical axis wind turbine in consideration of high angle of attack flow," *Renewable Energy*, vol. 51, pp. 317–330, 2013.

[25] A. Bianchini, F. Balduzzi, G. Ferrara, and L. Ferrari, "Aerodynamics of darrieus wind turbines airfoils: The impact of pitching moment," *Journal of Engineering for Gas Turbines and Power*, vol. 139, 10 2016.

[26] K. McLaren, "A numerical and experimental study of unsteady loading of high solidity vertical axis wind turbines," Ph.D. dissertation, McMaster University Hamilton, Ontario, 01 2011.

[Online]. Available: https://macsphere.mcmaster.ca/handle/11375/11096
[27] B. K. Kirke and L. Lazauskas, "Limitations of fixed pitch darrieus hydrokinetic turbines and the challenge of variable pitch," *Renewable Energy*, vol. 36, no. 3, pp. 893–897, 2011.